ATP release through connexin hemichannels and gap junction transfer of second messengers propagate Ca^{2+} signals across the inner ear

Fabio Anselmi[a], Victor H. Hernandez[a], Giulia Crispino[a], Anke Seydel[a], Saida Ortolano[a,b], Stephen D. Roper[c], Nicoletta Kessaris[d], William Richardson[d], Gesa Rickheit[e], Mikhail A. Filippov[f,1], Hannah Monyer[f], and Fabio Mammano[a,b,2]

[a]Foundation for Advanced Biomedical Research, Venetian Institute of Molecular Medicine, 35129 Padua, Italy; [b]Department of Physics ''G. Galilei,'' University of Padua, 35129 Padua, Italy; [c]Department of Physiology and Biophysics and Program in Neurosciences, Miller School of Medicine, University of Miami, Miami, FL 33136; [d]Wolfson Institute for Biomedical Research and Department of Biology, University College London, London WC1E 6BT, United Kingdom; [e]Leibniz-Institut für Molekulare Pharmakologie (FMP) and Max-Delbrück-Centrum für Molekulare Medizin (MDC), D-13125 Berlin, Germany; and [f]Department of Clinical Neurobiology, University Hospital of Neurology, Heidelberg, Germany

Edited by Michael V. L. Bennett, Albert Einstein College of Medicine, Bronx, NY, and approved September 12, 2008 (received for review January 28, 2008)

Extracellular ATP controls various signaling systems including propagation of intercellular Ca^{2+} signals (ICS). Connexin hemichannels, P2x7 receptors (P2x7Rs), pannexin channels, anion channels, vesicles, and transporters are putative conduits for ATP release, but their involvement in ICS remains controversial. We investigated ICS in cochlear organotypic cultures, in which ATP acts as an IP_3-generating agonist and evokes Ca^{2+} responses that have been linked to noise-induced hearing loss and development of hair cell-afferent synapses. Focal delivery of ATP or photostimulation with caged IP_3 elicited Ca^{2+} responses that spread radially to several orders of unstimulated cells. Furthermore, we recorded robust Ca^{2+} signals from an ATP biosensor apposed to supporting cells outside the photostimulated area in WT cultures. ICS propagated normally in cultures lacking either P2x7R or pannexin-1 (Px1), as well as in WT cultures exposed to blockers of anion channels. By contrast, Ca^{2+} responses failed to propagate in cultures with defective expression of connexin 26 (Cx26) or Cx30. A companion paper demonstrates that, if expression of either Cx26 or Cx30 is blocked, expression of the other is markedly downregulated in the outer sulcus. Lanthanum, a connexin hemichannel blocker that does not affect gap junction (GJ) channels when applied extracellularly, limited the propagation of Ca^{2+} responses to cells adjacent to the photostimulated area. Our results demonstrate that these connexins play a dual crucial role in inner ear Ca^{2+} signaling: as hemichannels, they promote ATP release, sustaining long-range ICS propagation; as GJ channels, they allow diffusion of Ca^{2+}-mobilizing second messengers across coupled cells.

deafness | mouse models | P2x7 receptor | pannexin | biosensor cells

In the organ of Corti, a polarized neurosensory epithelium of the inner ear (1) [supporting information (SI) *Text* and Fig. S1], non-sensory epithelial and supporting cells form a glial-like syncytium (2) interconnected by connexin 26 (Cx26) and Cx30, two connexins that may assemble to form heteromeric gap junction (GJ) channels (3). In several systems coupled by GJ channels, including retina glial cells and astrocytic networks, the spread of intercellular Ca^{2+} signals (ICS) provides a mechanism by which cooperative cell activity is thought to be coordinated (4, 5). Nanomolar levels of ATP on the apical surface of the organ of Corti, which have been linked to sound exposure (6), activate G protein-coupled $P2Y_2$ and $P2Y_4$ receptors (7, 8). Moreover, focal mechanical stimuli that release ATP evoke IP_3-dependent ICS that propagate radially across this cochlear cellular network at a uniform and constant speed of 10 to 15 μm/s (7, 8), comparable to the speed of glial Ca^{2+} waves (4, 5). ICS propagation across the organ of Corti is reduced by apyrase, suramin, or intracellular acidification in CO_2-saturated buffer (7, 9). The mechanisms that underlie cochlear ICS propagation (7–9), as well as spontaneous ATP release in the Kölliker organ before the onset of hearing (10), are consistent with Ca^{2+}-activated ATP release through unpaired connexons (11), i.e., non-junctional Cx hemichannels (12, 13). Indeed, increase of cytoplasmic free Ca^{2+} concentration ($[Ca^{2+}]_i$) triggers Cx hemichannel opening (14, 15), and functional studies in expression systems indicate that Cx26 and Cx30 may operate as hemichannels in the plasma membrane (16–18). Furthermore, ATP is released in an actin- and phospholipase-C-dependent manner through Cx hemichannels in HeLa cell cultures stably expressing human Cx26 (19). Finally, deafness-linked mutations of Cx26 that result in abnormally open hemichannels cause cell death (20), whereas unregulated ATP release through Cx30 hemichannels has been implicated in alteration of epidermal factors leading to a rare skin disorder (21).

However, it has been pointed out that most studies implicating Cx hemichannels relied on the use of pharmacological compounds that are not specific and have been shown to affect the activity of various other channels (22). Therefore, alternative conduits for ATP release, like the P2x7 receptor (P2x7R) (23, 24), which is expressed in the immature inner ear (25), and its co-immunoprecipitating partner Px1 (26), cannot be excluded based solely on responses to pharmacological inhibitors or mimetic peptides (22, 27). Matters are further complicated by the fact that ICS can be also transmitted by the direct transfer of Ca^{2+}-mobilizing second messengers from the cytosol of one cell to that of an adjacent one through GJ channels (28). Indeed, GJ-mediated transmission of Ca^{2+} waves was the first pathway identified in astrocytes (29). Interestingly, ICS propagation across heteromeric GJ channels consisting of Cx26 and Cx30 is reported to be faster than across their homomerically assembled counterparts (30). Furthermore, heteromeric mixing of different connexin isoforms, producing variation in channel stoichiometry and/or arrangements of isoforms within the hemichannels, may allow cells to

Author contributions: F.A. and F.M. designed research; F.A., V.H.H., G.C., A.S., S.O., G.R., and F.M. performed research; S.D.R., N.K., W.D.R., M.A.F., and H.M. contributed new reagents/analytic tools; F.A. and F.M. analyzed data; and F.A. and F.M. wrote the paper.

The authors declare no conflict of interest.

This article is a PNAS Direct Submission.

[1]Present address: Institute of Pharmacy and Biotechnology, Heidelberg University, 69120 Heidelberg, Germany.

[2]To whom correspondence should be addressed. E-mail: fabio.mammano@unipd.it.

This article contains supporting information online at www.pnas.org/cgi/content/full/0800793105/DCSupplemental.

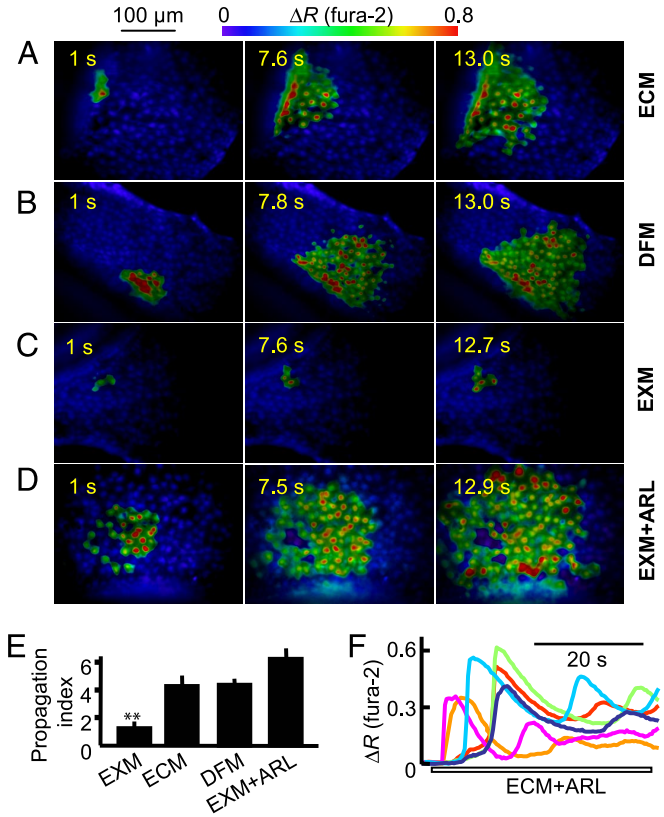

Fig. 1. Effect of divalent ions and ectonucleotidases on ICS evoked by ATP puffs in the organ of Corti. (*A-D*) Representative experiments showing pseudocolor images of Ca^{2+} signals (measured as fura-2 emission ratio changes; ΔR) propagating through cochlear supporting and epithelial cells of P3-P6 mouse organotypic cultures following focal delivery of an ATP puff (50 ms, 4 μM) from a glass micropipette with a tip opening of $\approx$1.5 μm. EXM, extracellular medium containing 2 mM Ca^{2+}; ECM, medium containing endolymphatic Ca^{2+} concentration (20 μM); DFM, medium devoid of divalent ions; EXM+ARL, ectonucleotidase inhibitor ARL67156 (100 μM) dissolved in EXM. Time of image capture measured from the end of ATP delivery is indicated on each frame. (*E*) Pooled data showing ICS propagation index for conditions in *A-D*; data are mean $\pm$ SEM for independently repeated experiments on at least five cultures from different animals; $^{**}P < 0.01$, Student *t* test. (*F*) Representative whole-cell averages of fura-2 ΔR versus time for randomly selected cells in a culture bathed in ECM and stimulated with 100 μM ARL67156 (empty bar at bottom marks timing of drug delivery).

regulate their intercellular communication properties, including molecular selectivity to inositol phosphates (31). Permeability to IP_3 is impaired in a deafness mutant of Cx26 (9).

By using focal ATP delivery (8) or photostimulation with caged IP_3 (32), we have performed accurate measurements of cochlear ICS propagation range, hereby defined as the ratio between the culture area invaded by Ca^{2+} signals and the area responding within 1 s to the applied stimulus (i.e., ATP puff or laser radiation). A value of 1 indicates no propagation (see *SI Text*). We show that Ca^{2+} signals fail to propagate in cultures with deficient expression of Cx26 and Cx30, whereas ICS in cultures from mice lacking Px1 or P2x7R are indistinguishable from those of WT controls.

Vesicular- and transporter-mediated release was not investigated in this study, as (*i*) vesicular storage of ATP has been detected in the cochlear lateral wall but not in cells of the organ of Corti (6, 33), and (*ii*) previous work has shown that blockage of either vesicular ATP release or ATP-binding cassette transporters fails to inhibit ATP release (11).

Results

Divalent Ions and Ectonucleotidases Control Ca^{2+} Signaling in WT Cochlear Cultures. In the first set of experiments (Fig. 1), we loaded cochlear organotypic cultures with the AM ester moiety of the Ca^{2+} indicator fura-2 and measured ICS in supporting and epithelial cells stimulated with ATP puffs (50 ms, 4 μM) delivered from a glass micropipette located above the outer hair cell region (Fig. S1) as previously described (7, 8). *In vivo*, the apical surface of the cochlear sensory epithelium is bathed in endolymph, an unusual extracellular fluid containing 150 mM K^+, 2 mM Na^+, and as little as 20 μM extracellular free Ca^{2+} concentration ($[Ca^{2+}]_o$) (34). We tested ICS propagation in ECM, a medium with endolymph-like $[Ca^{2+}]_o$ (Fig. 1*A* and Movie S1), or DFM, a medium devoid of divalent ions (Fig. 1*B*), and in both cases we obtained ICS similar to those evoked by focal mechanical stimuli (7, 8). ICS range decreased significantly in EXM, an extracellular medium containing 2 mM $[Ca^{2+}]_o$ (Fig. 1*C*). However, in EXM supplemented with the ectonucleotidase inhibitor ARL67156 (100 μM), the ICS range was similar to that measured in ECM (Fig. 1*D*; pooled data are shown in Fig. 1*E*), suggesting that EXM presumably reduces hemichannel basal opening, but the ATP that is released in the presence of ARL67156 is enough to support ICS propagation. Consistent with this hypothesis, in ECM supplemented with ARL67156 (100 μM), we recorded the spontaneous (i.e., unstimulated) occurrence of Ca^{2+} oscillations (Fig. 1*F*) similar to those elicited by extracellular ATP in concentrations ranging between 20 nM and $\approx$1 μM (7, 8). These results highlight the sensitivity of cochlear supporting cell Ca^{2+} signaling to $[Ca^{2+}]_o$ and ATP degradation by ectonucleotidases expressed at the endolymphatic surface of the organ of Corti (35, 36).

Ca^{2+} Signals Fail to Propagate in Connexin-Deficient Cochlear Cultures. By using antibodies against Cx26 extracellular loop peptides (18), we detected immunofluorescence signals near the apex of fixed, but not permeabilized, cochlear supporting and epithelial cells (Fig. S2), suggesting that unpaired connexons may be present in the apical plasma membrane, which prompted us to further test the hypothesis that Cx hemichannels release ATP in this system.

Thus, in the second set of experiments (Fig. 2), we co-loaded cochlear organotypic cultures from WT or transgenic mice with the AM esters of fura red (a visible light-excitable fura-2 analogue) and caged IP_3. By focusing UV laser light (100 ms, 375 nm) within a well defined area in the organ of Corti bathed in ECM, we photostimulated supporting cells containing caged IP_3, effectively bypassing the initial activation of P2Y receptors by extracellular ATP. In WT cultures, focal IP_3 uncaging elicited ICS that spread radially to several orders of unirradiated cells (Fig. 2*A* and Movie S2). ICS propagation was hampered in cultures lacking Cx26 (Fig. 2*B* and Movie S3) or Cx30 (Fig. 2*C*), but normal in cultures lacking either P2x7R (Fig. 2*D*) or Px1 (Fig. 2*E*). Pooled data are shown in Fig. 2 *F* and *G*. Sensitivity of Ca^{2+} responses to $[Ca^{2+}]_o$ and ectonucleotidases was similar in WT, P2x7R KO, and Px1 KO cultures (Fig. S3). Furthermore, the purinergic signaling cascade (7, 8) was intact in these experiments, as all cultures responded to extracellular ATP with the expected pattern of Ca^{2+} oscillations (not shown). The selective P2x7R inhibitor brilliant blue G and anion channel inhibitors SITS, DIDS, tamoxifen, and glybenclamide had no effect on ICS propagation in ECM (Fig. S4*A*), whereas ICS spread was inhibited in ECM supplemented with the nonselective Cx channel blockers CBX (in a dose-dependent manner), niflumic acid (200 μM), and flufenamic acid (50 μM) (Fig. S4*B*). Taken together, these experiments clearly show that connexins are involved in the process of ICS propagation illustrated in Fig. 2.

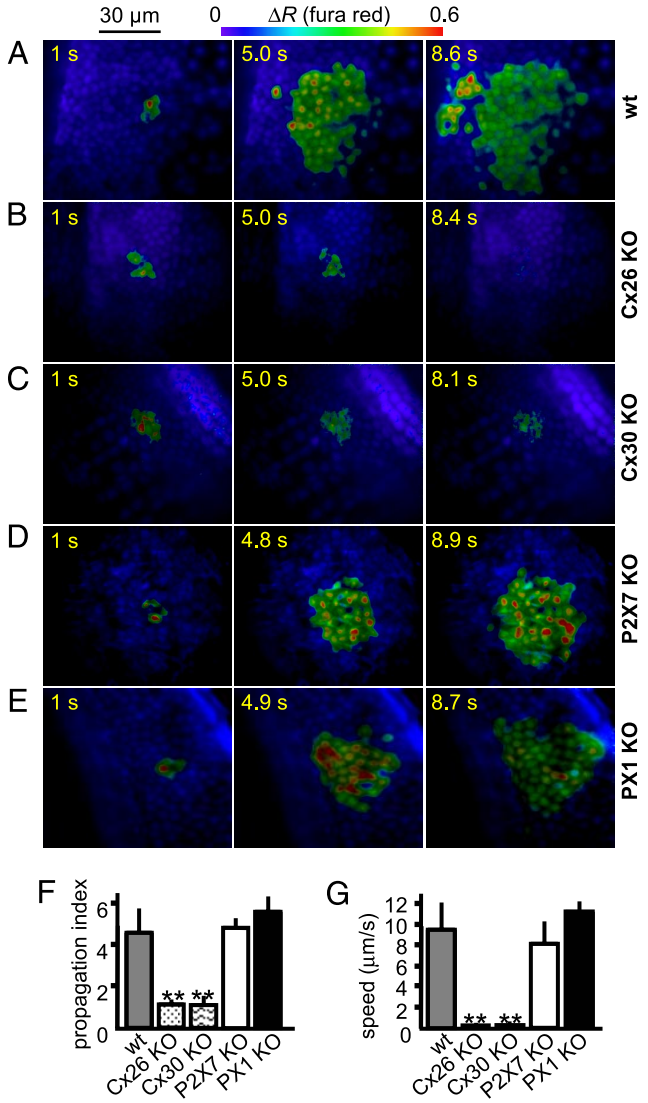

Fig. 2. Ca^{2+}signals evoked by 100 ms of focal photostimulation with caged IP_3 fail to propagate in connexin-deficient cochlear cultures but propagate normally in Px1 KO and P2x7 KO cultures. (*A-E*) Ca^{2+} signals in cochlear supporting and epithelial cells from P3-P6 mouse organotypic cultures bathed in ECM and co-loaded with the AM esters of fura red and caged IP_3. (*A*) Control (WT culture); (*B*) Cx26 KO culture; (*C*) Cx30 KO culture; (*D*) P2x7 KO culture; (*E*) Px1 KO culture. (*F*) Pooled data showing propagation range in WT controls and in cultures lacking Cx26, Cx30, P2x7, or Px1. (*G*) Speed of propagating ICS for data in *F*. Data in *F* and *G* are mean ± SEM for independently repeated experiments in tissues from at least three different animals.

Photostimulation with Caged IP_3 Releases ATP to the Extracellular Medium. To investigate the relationship between photorelease of caged IP_3, ATP release, and Cx hemichannels, we performed a third set of experiments using cellular biosensors (37) (Fig. 3). ATP biosensor responses are mediated by Ca^{2+} influx through P2x2 and P2x3 ionotropic receptors (37); therefore, data were collected in an extracellular medium containing 100 μM Ca^{2+}, a concentration that does not impair ICS propagation in WT cultures. We separately preloaded ATP biosensors with fluo-4AM and cochlear cultures with caged IP_3 AM. When a pipette-held ATP biosensor was apposed to a supporting cell outside the UV exposed area in a WT culture (Fig. 3 *A* and *B*), we reliably recorded robust biosensor Ca^{2+} signals (Fig. 3*C*). We failed to detect similar signals following IP_3 uncaging in Cx26 KO or Cx30 KO cultures (not shown). We note in passing that ICS propagated to cells in the Kölliker organ following IP_3 uncaging in Hensen cells of WT cultures bathed in ECM (Fig. S5 and Movie S4). Thus, ATP release through Cx hemichannels allows communication across supporting cells in the two separate GJ-coupled compartments (38) that are found on opposite sides of the sensory hair cell region, as well as within each one of these compartments.

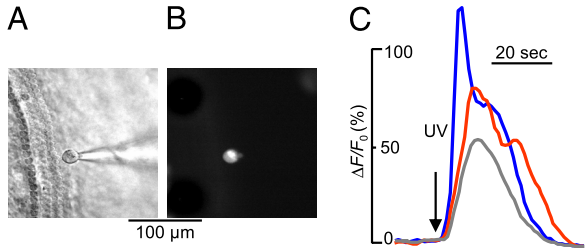

Fig. 3. Ca^{2+}responses evoked in ATP biosensors by 100 ms of focal photostimulation of cochlear supporting cells with caged IP_3. (*A*) Example of a pipette-held biosensor loaded with fluo-4 and apposed to a Hensen's cell in a culture loaded with caged IP_3 AM and viewed with bright-field differential interference contrast optics. (*B*) The same field under conventional epifluorescence illumination. (*C*) Representative biosensor whole-cell pixel averages of percent fluo-4 fluorescence change (ΔF) relative to pre-stimulus fluorescence emission intensity (F_0) measured before delivery of the photostimulation (arrow, stimulus onset), versus time for similar independently repeated experiments performed in tissues from three different animals.

Diffusion and Efflux of Calcein from Cochlear Supporting Cells. As cochlear Cx hemichannels release ATP, a charged and relatively large molecule (MW 340, charge −4 at physiological pH [39]), they might also release fluorescent tracers with similar charge and size. Calcein, which has approximately six negative and two positive charges at pH 7 (MW 622, net charge −4) is a polyanionic fluorescein derivative that, according to the manufacturer, exhibits fluorescence essentially independent of pH between 6.5 and 12. Thus, in the fourth set of experiments (Fig. 4 and Figs. S6–S8), we initially verified that calcein diffuses across GJ channels in the organ of Corti of WT cochlear cultures (Fig. S6). Thereafter, we assayed calcein efflux from cochlear cultures bathed in ECM and preloaded with the AM moiety of this tracer (Fig. 4). In particular, we compared calcein efflux rates in WT, Cx26 KO, and Cx30 KO cultures and we also tested the effects of CBX and lanthanum (La^{3+}). The latter has been reported to block IP_3-triggered ATP release in a rat brain endothelial cell line (40). La^{3+} also impairs dye uptake in rat cortical astrocytes expressing Cx43 (41) and blocks hemichannel currents evoked by depolarization of HeLa cells transfected with cDNA encoding rat Cx43 (42). We recorded hemichannel currents evoked by

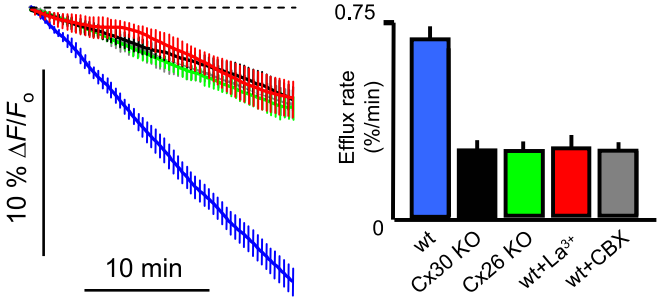

Fig. 4. Calcein efflux from supporting cells of the organ of Corti. *Left*, time course of percent fluorescence emission change (ΔF) relative to initial fluorescence intensity (F_0) in cultures preloaded with calcein AM. *Right*, efflux rate from data at left. Values shown as mean ± SEM for independently repeated experiments on cultures from at least four different animals.

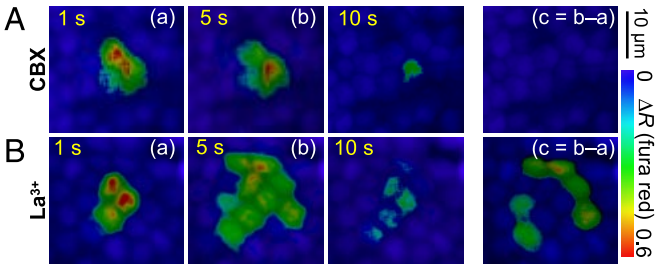

Fig. 5. Effects of CBX and La^{3+} on the spread of Ca^{2+} signals evoked by 100 ms of photostimulation with caged IP_3 in the organ of Corti. Ca^{2+} responses of cultures incubated with 100 μM CBX (*A*) or 100 μM La^{3+} (*B*). The fourth image in each sequence is the pixel-by-pixel difference (i.e., c = b − a) of the first two images. Results are representative of similar independently repeated experiments performed in tissues from at least three different animals.

depolarization in patch-clamped solitary HeLa cells transiently transfected with mouse Cx30 (16) tagged with a color variant of the GFP (43), and we determined that La^{3+} (100 μM) blocks these currents (Fig. S8). Addition of La^{3+} (100 μM) to ECM markedly reduced calcein efflux from WT cochlear cultures (Fig. 4). Indeed, in WT cultures exposed to La^{3+} (100 μM) or CBX (100 μM), calcein efflux rate was comparable to that of Cx26 KO or Cx30 KO cultures bathed in ECM but not exposed to any drug (Fig. 4). The residual efflux in the connexin KOs and in La^{3+} or CBX may be a result of dye loss (which may be tracer-dependent) through the membrane or other uncharacterized pathways. However, in gap-fluorescence recovery after photobleaching assays (44), calcein fluorescence recovery after photobleaching in WT cultures exposed to La^{3+} (100 μM) was similar to controls, whereas no recovery was observed in WT cultures exposed to CBX (100 μM; Fig. S7). Fluorescence recovery after photobleaching occurs by dye permeation through cell-cell channels, which partially restores the dye's intracellular pool within the photobleached cells. Incomplete recovery of fluorescence intensity is ascribed to the fraction of the pool that is not available for intercellular transfer, as a result of trapping into subcellular organelles and/or binding to subcellular structures (45). Thus, our experiments (Fig. 4 and Figs. S6–S8) clearly indicate that membrane-permeable CBX blocks both Cx hemichannels and GJ channels, whereas La^{3+} blocks Cx hemichannels but has no access to intercellular channels in GJ plaques. In summary, based on the experiments described so far and our previous work (7, 8), we conclude that Ca^{2+} signals can be transmitted across cochlear supporting and epithelial cells via extracellular diffusion of a signaling molecule, ATP, which is released through Cx hemichannels and acts on G protein-coupled $P2Y_2$ and $P2Y_4$ receptors (7, 8).

Diffusion of Ca^{2+}-Mobilizing Second Messengers Through GJ Channels. To investigate the relationship between ICS propagation and GJ channels, in the last series of experiments we exploited the different blocking characteristics of CBX and La^{3+} highlighted earlier. Thus, in cultures bathed in ECM co-loaded with caged IP_3 and fura red, uncaging IP_3 in the presence of CBX (100 μM) evoked Ca^{2+} signals that remained confined within the UV-irradiated area (Fig. 5*A*). In the presence of La^{3+} (100 μM), Ca^{2+} signal spread to first-order cells, i.e., cells adjacent to the irradiated area (Fig. 5*B*). The results in Fig. 5*B* are consistent with those obtained by directly injecting IP_3 in a single supporting cell while inhibiting P2Y receptors with suramin (9). Thus, we ascribe the spread of Ca^{2+} signals in Fig. 5*B* to the direct diffusion of Ca^{2+}-mobilizing second messengers, most likely IP_3 (9), through GJ channels.

Discussion

In this article we investigated the mechanisms underlying ICS propagation across epithelial and supporting cells of the organ of Corti challenged with extracellular ATP puffs or photostimulated with caged IP_3. Non-sensory cells of the cochlear epithelium express the intermediate filament glial fibrillary acidic protein, a classic marker for astrocytes (2), and are thought to perform similar spatial buffering of K^+, the major charge carrier implicated in mechano-electrical transduction (3, 46, 47). Activation of Cx43 hemichannels in the astrocyte plasma membrane causes the release of ATP into the extracellular space (48), where it activates P2Y receptors on adjacent cells to initiate a Ca^{2+} wave (12, 13).

In addition, Px1 and P2x7R have been implicated in ATP secretion from glial cells during Ca^{2+} wave propagation (49) and amplification of astrocytic ICS (24). Px1 can assemble in the plasma membrane (50, 51), forming mechano-sensitive conduits that are permeable to ATP (52) and underlie ATP release from erythrocytes challenged by mechanical stretch (53), as well as mouse taste receptors activated by gustatory stimuli (37). However, determining the exact function for pannexons and how they differ from connexons has been so far undermined by lack of specific channel blocker and Px gene KO animals (54). Furthermore, interactions between Px1 and P2x7R have been documented. In particular, co-expression of Px1 and P2x7R produces a signaling complex that, when activated by ATP, leads to opening of a cation channel, the creation of a transmembrane pathway sufficiently large to allow the passage of large molecular weight fluorescent dyes (up to 900 Da), and cell lysis (26, 55). The large-pore permeation properties of the P2x7R/Px1 complex are greatly enhanced by removal of divalent cations and inhibited by CBX (55) whereas, in the absence of Px1, P2x7R behaves like a simple cation channel that is resistant to treatment with CBX and other nonselective connexin channel blockers (26, 55, 56).

Our results with caged IP_3 and genetically targeted mice overcome ambiguities resulting from a lack of specific channel blockers, demonstrating that ICS propagate normally in cultures lacking either P2x7R or Px1, but fail to propagate in cultures with defective expression of Cx26 or Cx30. We thus exclude that channels composed of Px1, P2x7R, or a combination of the two play a significant role. Besides P2x7R (25), the only P2X-type receptor that has been detected consistently in epithelial, supporting, and sensory cells of the rat organ of Corti is the P2x2R (57). In the developing cochlea, at P6 (an age pertinent to our studies), Hensen's cells, Deiters' and inner phalangeal cell processes, and Claudius cells, all express P2x2R (57). However, we did not detect significant differences in ICS propagation using DFM or ECM, consistent with the fact that ATP-gated ion currents recorded from cochlear supporting cells activate at ATP concentrations in excess of 10 μM (58). By contrast, based on the comparison of our fura-2 Ca^{2+} signals in Fig. 1 to the ATP dose-response curve in figure 2 of Gale et *al.* (7), we estimate that ATP levels stay in the sub-micromolar range during ICS propagation in the organ of Corti. Hence we exclude P2x2R contributions to the Ca^{2+} signals presented in this article.

Anion channel inhibitors had no effect on ICS propagation in ECM (Fig. S4A), whereas, as mentioned earlier in this article, contributions from vesicular- and transporter-mediated ATP release can be excluded based on previous work (11). Therefore, based on evidence presented in this article and in our previous work (7–9), we conclude that connexins afford two concurrent pathways by which ICS propagate across the organ of Corti; one involves release of ATP through Cx hemichannels and its diffusion in the extracellular space, coupled to activation of $P2Y_2$ and $P2Y_4$ membrane receptors that are responsive to nanomolar ATP in this system (7, 8); the other involves the transfer of

CELL BIOLOGY

Ca^{2+}-mobilizing signaling molecules, and possibly also other types of second messengers (59), directly from the cytosol of one cell to that of an adjacent cell through GJ channels (9).

The unique composition of endolymph makes ATP release through Cx hemichannels an attractive candidate for ICS propagation *in vivo*, as low endolymphatic $[Ca^{2+}]_o$ (34) is expected to bias Cx hemichannels in the apical plasma membrane toward the open state (60). Another important factor that may contribute to enhancing hemichannel activity in cells exposed to endolymph is the high level of endolymphatic K^+ (61). Frequency and duration of Cx hemichannel opening may be additionally regulated by physiological intracellular triggers, most notably intracellular Ca^{2+} (14, 15). Thus, work performed on Cx32-expressing cells showed that an increase in $[Ca^{2+}]_i$ triggers ATP release (and dye uptake) that is critically dependent on $[Ca^{2+}]_i$ elevation within a concentration "window" situated around 500 nM (see figs. 7 *E* and *F* of ref. 14). Although we have not performed a similar characterization of $[Ca^{2+}]_i$-dependent ATP release, it is interesting to note that ICS mobilize $[Ca^{2+}]_i$ to peak levels of $\approx$500 nM in our system (7, 9).

Complete blockade of ICS propagation in cochlear cultures lacking either Cx26 or Cx30 is not entirely unexpected, as a substantial decrease in Cx26 protein level (but not mRNA) was recently reported in cochlea of Cx30 KO mice (62). Likewise, the amount of Cx26 protein in liver cells of Cx32 KOs is significantly lower than in controls (63). We analyzed this phenomenon in detail and, in a companion article, we provide evidence for coordinated regulation of inner ear Cx26 and Cx30 expression, at both the mRNA and the protein level, as a result of signaling through phospholipase C and NFκB pathway in cochlear supporting and epithelial cells in a region between the outer hair cells and the stria vascularis. However, other unexplored facets call for further analyses. Indeed, in our opinion, one of the main goals for future research is certainly that of achieving a clearer picture of intercellular signaling in the inner ear.

Materials and Methods

Organ Cultures. Cochleae were dissected from P3-P6 mouse pups in ice-cold Hepes-buffered (10 mM, pH 7.2) Hanks' balanced salt solutions (HBSS; Sigma) and placed onto glass coverslips coated with 10 g/ml of Cell Tak (Becton Dickinson), as described by Gale *et al.* (7). Cultures were incubated in DMEM/F12 (Invitrogen), supplemented with FBS 5% and maintained at 37 °C for 1 d. For experiments, cultures were superfused at 2 ml/min with an extracellular medium (i.e., EXM) containing 138 mM NaCl, 5 mM KCl, 2 mM $CaCl_2$, 0.3 mM NaH_2PO_4, 0.4 mM KH_2PO_4, 10 mM Hepes-NaOH, and 6 mM d-glucose (pH 7.2; 320 mOsm). ECM refers to a similar medium with a reduced Ca^{2+} concentration of 20 μM. DFM refers to a similar medium devoid of divalent ions. Experiments were performed at room temperature, 22 °C-24 °C. For further methodological details, see the *SI Text*.

ACKNOWLEDGMENTS. The authors thank GlaxoSmithKline Services Unlimited for the P2x7 KO mice; Klaus Willecke for the $Cx26^{loxP/loxP}$ and Cx30 KO mice; Guy Tran Van Nhieu for the generous gift of antibodies against Cx26 extracellular loop peptides; Thomas J. Jentsch for discussions and support for Gesa Rickheit; and Tullio Pozzan, Pierluigi Nicotera, Francesco Di Virgilio, Roberto Bruzzone, and the editor of this article, Michael V.L. Bennett, for discussions and constructive criticism. This work was funded by a grant from Fondazione Cariparo/Progetti di Eccellenza 2006 (F.M.), grant GGP05131 from Telethon Italy, and grant LSHGCT20054512063 from the European Commission FP6 Integrated Project EuroHear under the Sixth Research Frame Program of The European Union. Funding for biosensor cells was provided by National Institutes of Health/National Institute on Deafness and Other Communication Disorders grant DC007630 (to S.D.R.).

1. Krstic RV (1997) *Human Microscopic Anatomy*. (Springer-Verlag, Berlin).
2. Rio C, Dikkes P, Liberman MC, Corfas G (2002) Glial fibrillary acidic protein expression and promoter activity in the inner ear of developing and adult mice. *J Comp Neurol* 442:156–162.
3. Zhao HB, Kikuchi T, Ngezahayo A, White TW (2006) Gap junctions and cochlear homeostasis. *J Membr Biol* 209:177–186.
4. Metea MR, Newman EA (2006) Calcium signaling in specialized glial cells. *Glia* 54:650–655.
5. Scemes E, Giaume C (2006) Astrocyte calcium waves: what they are and what they do. *Glia* 54:716–725.
6. Munoz DJ, Kendrick IS, Rassam M, Thorne PR (2001) Vesicular storage of adenosine triphosphate in the guinea-pig cochlear lateral wall and concentrations of ATP in the endolymph during sound exposure and hypoxia. *Acta Otolaryngol* 121:10–15.
7. Gale JE, Piazza V, Ciubotaru CD, Mammano F (2004) A mechanism for sensing noise damage in the inner ear. *Curr Biol* 14:526–529.
8. Piazza V, Ciubotaru CD, Gale JE, Mammano F (2007) Purinergic signalling and intercellular Ca^{2+} wave propagation in the organ of Corti. *Cell Calcium* 41:77–86.
9. Beltramello M, Piazza V, Bukauskas FF, Pozzan T, Mammano F (2005) Impaired permeability to $Ins(1,4,5)P_3$ in a mutant connexin underlies recessive hereditary deafness. *Nat Cell Biol* 7:63–69.
10. Tritsch NX, Yi E, Gale JE, Glowatzki E, Bergles DE (2007) The origin of spontaneous activity in the developing auditory system. *Nature* 450:50–55.
11. Zhao HB, Yu N, Fleming CR (2005) Gap junctional hemichannel-mediated ATP release and hearing controls in the inner ear. *Proc Natl Acad Sci USA* 102:18724–18729.
12. Bennett MVL, Contreras JE, Bukauskas FF, Saez JC (2003) New roles for astrocytes: gap junction hemichannels have something to communicate. *Trends Neurosci* 26:610–617.
13. Goodenough DA, Paul DL (2003) Beyond the gap: functions of unpaired connexon channels. Nat Rev *Mol Cell Biol* 4:285–294.
14. De Vuyst E, *et al.* (2006) Intracellular calcium changes trigger connexin 32 hemichannel opening. *EMBO J* 25:34–44.
15. Pearson RA, Dale N, Llaudet E, Mobbs P (2005) ATP released via gap junction hemichannels from the pigment epithelium regulates neural retinal progenitor proliferation. *Neuron* 46:731–744.
16. Valiunas V, Weingart R (2000) Electrical properties of gap junction hemichannels identified in transfected HeLa cells. *Pflugers Arch* 440:366–379.
17. Gonzalez D, Gomez-Hernandez JM, Barrio LC (2006) Species specificity of mammalian connexin-26 to form open voltage-gated hemichannels. *FASEB J* 20:2329–2338.
18. Clair C, Combettes L, Pierre F, Sansonetti P, Tran Van Nhieu G (2008) Extracellular-loop peptide antibodies reveal a predominant hemichannel organization of connexins in polarized intestinal cells. *Exp Cell Res* 314:1250–1265.
19. Tran Van Nhieu G, Clair C, Bruzzone R, Mesnil M, Sansonetti P, Combettes L (2003) Connexin-dependent inter-cellular communication increases invasion and dissemination of Shigella in epithelial cells. *Nat Cell Biol* 5:720–726.
20. Stong BC, Chang Q, Ahmad S, Lin X (2006) A novel mechanism for connexin 26 mutation linked deafness: cell death caused by leaky gap junction hemichannels. *Laryngoscope* 116:2205–2210.
21. Essenfelder GM, *et al.* (2004) Connexin30 mutations responsible for hidrotic ectodermal dysplasia cause abnormal hemichannel activity. *Hum Mol Genet* 13:1703–1714.
22. Spray DC, Ye ZC, Ransom BR (2006) Functional connexin "hemichannels": a critical appraisal. *Glia* 54:758–773.
23. Pellegatti P, Falzoni S, Pinton P, Rizzuto R, Di Virgilio F (2005) A novel recombinant plasma membrane-targeted luciferase reveals a new pathway for ATP secretion. *Mol Biol Cell* 16:3659–3965.
24. Suadicani SO, Brosnan CF, Scemes E (2006) P2X7 receptors mediate ATP release and amplification of astrocytic intercellular Ca^{2+} signaling. *J Neurosci* 26:1378–1385.
25. Nikolic P, Housley GD, Thorne PR (2003) Expression of the P2X7 receptor subunit of the adenosine 5′-triphosphate-gated ion channel in the developing and adult rat cochlea. *Audiol Neurootol* 8:28–37.
26. Pelegrin P, Surprenant A (2006) Pannexin-1 mediates large pore formation and interleukin-1beta release by the ATP-gated P2X7 receptor. *EMBO J* 25:5071–5082.
27. Wang J, Ma M, Locovei S, Keane RW, Dahl G (2007) Modulation of membrane channel currents by gap junction protein mimetic peptides: size matters. *Am J Physiol Cell Physiol* 293:C1112–C1119.
28. Saez JC, Connor JA, Spray DC, Bennett MVL (1989) Hepatocyte gap junctions are permeable to the second messenger, inositol 1,4,5-trisphosphate, and to calcium ions. *Proc Natl Acad Sci USA* 86:2708–2712.
29. Finkbeiner S (1992) Calcium waves in astrocytes-filling in the gaps. *Neuron* 8:1101–1108.
30. Sun J, *et al.* (2005) Cochlear gap junctions coassembled from Cx26 and 30 show faster intercellular Ca^{2+} signaling than homomeric counterparts. *Am J Physiol Cell Physiol* 288:C613–C623.
31. Ayad WA, Locke D, Koreen IV, Harris AL (2006) Heteromeric, but not homomeric, connexin channels are selectively permeable to inositol phosphates. *J Biol Chem* 281:16727–16739.
32. Leybaert L, Sanderson MJ (2001) Intercellular calcium signaling and flash photolysis of caged compounds: a sensitive method to evaluate gap junctional coupling. *Methods Mol Biol* 154:407–430.
33. White PN, *et al.* (1995) Quinacrine staining of marginal cells in the stria vascularis of the guinea-pig cochlea: a possible source of extracellular ATP? *Hear Res* 90:97–105.
34. Bosher SK, Warren RL (1978) Very low calcium content of cochlear endolymph, an extracellular fluid. *Nature* 273:377–378.
35. Housley GD, *et al.* (2002) Purinergic regulation of sound transduction and auditory neurotransmission. *Audiol Neurootol* 7:55–61.
36. Vlajkovic SM, *et al.* (2004) Noise exposure induces up-regulation of ecto-nucleoside triphosphate diphosphohydrolases 1 and 2 in rat cochlea. *Neuroscience* 126:763–773.
37. Huang YJ, *et al.* (2007) The role of pannexin 1 hemichannels in ATP release and cell-cell communication in mouse taste buds. *Proc Natl Acad Sci USA* 104:6436–6441.

38. Jagger DJ, Forge A (2006) Compartmentalized and signal-selective gap junctional coupling in the hearing cochlea. *J Neurosci* 26:1260–1268.
39. Storer AC, Cornish-Bowden A (1976) Concentration of MgATP2- and other ions in solution. Calculation of the true concentrations of species present in mixtures of associating ions. *Biochem J* 159:1–5.
40. Braet K, *et al.* (2003) Pharmacological sensitivity of ATP release triggered by photoliberation of inositol-1,4,5-trisphosphate and zero extracellular calcium in brain endothelial cells. *J Cell Physiol* 197:205–213.
41. Contreras JE, *et al.* (2002) Metabolic inhibition induces opening of unapposed connexin 43 gap junction hemichannels and reduces gap junctional communication in cortical astrocytes in culture. *Proc Natl Acad Sci USA* 99:495–500.
42. Contreras JE, Saez JC, Bukauskas FF, Bennett MVL (2003) Gating and regulation of connexin 43 (Cx43) hemichannels. *Proc Natl Acad Sci USA* 100:11388–11393.
43. Beltramello M, *et al.* (2003) Permeability and gating properties of human connexins 26 and 30 expressed in HeLa cells. *Biochem Biophys Res Commun* 305:1024–1033.
44. Wade MH, Trosko JE, Schindler M (1986) A fluorescence photobleaching assay of gap junction-mediated communication between human cells. *Science* 232:525–528.
45. Rabut G, Ellenberg J (2005) Photobleaching techniques to study mobility and molecular dynamics of proteins in live cells: FRAP, iFRAP, and FLIP. *Live Cell Imaging*, ed Goldman RD, Spector DL (Cold Spring Harbor Lab Press, Cold Spring Harbor, NY), pp 101–126.
46. Hibino H, Kurachi Y (2006) Molecular and physiological bases of the K+ circulation in the mammalian inner ear. *Physiology (Bethesda)* 21:336–345.
47. Wangemann P (2006) Supporting sensory transduction: cochlear fluid homeostasis and the endocochlear potential. *J Physiol* 576:11–21.
48. Kang J, *et al.* (2008) Connexin 43 hemichannels are permeable to ATP. *J Neurosci* 28:4702–4711.
49. Barbe MT, Monyer H, Bruzzone R (2006) Cell-cell communication beyond connexins: the pannexin channels. *Physiology (Bethesda)* 21:103–4114.
50. Bruzzone R, Barbe MT, Jakob NJ, Monyer H (2005) Pharmacological properties of homomeric and heteromeric pannexin hemichannels expressed in Xenopus oocytes. *J Neurochem* 92:1033–1043.
51. Boassa D, *et al.* (2007) Pannexin1 channels contain a glycosylation site that targets the hexamer to the plasma membrane. *J Biol Chem* 282:31733–31743.
52. Bao L, Locovei S, Dahl G (2004) Pannexin membrane channels are mechanosensitive conduits for ATP. *FEBS Lett* 572:65–68.
53. Locovei S, Bao L, Dahl G (2006) Pannexin 1 in erythrocytes: function without a gap. *Proc Natl Acad Sci USA* 103:7655–7659.
54. Shestopalov VI, Panchin Y (2008) Pannexins and gap junction protein diversity. *Cell Mol Life Sci* 65:376–394.
55. Locovei S, Scemes E, Qiu F, Spray DC, Dahl G (2007) Pannexin1 is part of the pore forming unit of the P2X(7) receptor death complex. *FEBS Lett* 581:483–488.
56. Petrou S, Ugur M, Drummond RM, Singer JJ, Walsh JV Jr (1997) P2X7 purinoceptor expression in Xenopus oocytes is not sufficient to produce a pore-forming P2Z-like phenotype. *FEBS Lett* 411:339–345.
57. Jarlebark LE, Housley GD, Raybould NP, Vlajkovic S, Thorne PR (2002) ATP-gated ion channels assembled from P2X2 receptor subunits in the mouse cochlea. *Neuroreport* 13:1979–1984.
58. Lagostena L, Ashmore JF, Kachar B, Mammano F (2001) Purinergic control of intercellular communication between Hensen's cells of the guinea-pig cochlea. *J Physiol* 531:693–706.
59. Hernandez VH, *et al.* (2007) Unitary permeability of gap junction channels to second messengers measured by FRET microscopy. *Nat Methods* 4:353–358.
60. Saez JC, Retamal MA, Basilio D, Bukauskas FF, Bennett MVL (2005) Connexin-based gap junction hemichannels: gating mechanisms. *Biochim Biophys Acta* 1711:215–224.
61. Srinivas M, Calderon DP, Kronengold J, Verselis VK (2006) Regulation of connexin hemichannels by monovalent cations. *J Gen Physiol* 127:67–75.
62. Ahmad S, *et al.* (2007) Restoration of connexin26 protein level in the cochlea completely rescues hearing in a mouse model of human connexin30-linked deafness. *Proc Natl Acad Sci USA* 104:1337–1341.
63. Nelles E, *et al.* (1996) Defective propagation of signals generated by sympathetic nerve stimulation in the liver of connexin32-deficient mice. *Proc Natl Acad Sci USA* 93:9565–9570.

Supporting Information

Anselmi *et al.* 10.1073/pnas.0800793105

SI Text

Reagents and Drugs. Membrane permeable AM ester derivatives of fura-2, fura red, fluo-4, and calcein were obtained from Invitrogen/Molecular Probes. Membrane-permeable caged inositol (1, 4, 5) triphosphate (caged IP_3 AM) was purchased from Alexis. ATP, 4-acetamido-4′-isothiocyanostilbene-2,2′-disulfonate, 4,4′-di-isothiocyanatostilbene-2,2′-disulfonic acid, tamoxifen, glybenclamide, brilliant blue G, carbenoxolone, lanthanum chloride, niflumic acid, flufenamic acid, ARL67156, pluronic F-127, and sulfinpyrazone were purchased from Sigma.

Transgenic Mice and Genotyping. The background strains of the transgenic mice used in this study are as follows: Cx30 KO (1), mixed C57BL/6 and 129/Ola; $Cx26^{loxP/loxP}$ (2), mixed C57BL/6 and 129/SvPasCrl; Sox10-CRE (3), mixed BL6CBAF1 and 129/Sv; P2x7 KO (4), C57BL/6; Px1 KO (this article), C57BL/6.

The mouse Px1 gene was disrupted by inserting the lacZ gene and a phosphoglycerate kinase-neomycin cassette flanked by *loxP* sites into exon1 of the Px1 gene via homologous recombination. The DNA fragment used originated from a 129/SvJ mouse genomic library (Stratagene). The final targeting vector contained 3.0 and 5.0 kb of homologous sequence 5′ and 3′ of the inserted sequence. The targeting vector was linearized at a unique NotI site, and after electroporation of R1 embryonic stem cells, four positive clones were identified by nested PCR and confirmed by Southern blot analysis. Two clones were injected into blastocysts and implanted into foster mothers that gave birth to 15 highly chimeric animals. Germline transmission of the mutant allele was determined by Southern blot analysis. After the removal of the neomycin cassette by breeding with Cre-deleter mice, the mice were backcrossed to C57BL/6 mice. Breeding of heterozygous mice yielded Px1 KO mice at a Mendelian ratio.

Evidence for complete Px1 deletion was obtained by RT-PCR analysis on brain tissue from 5 month old mice with the following primers: Px1ex3-F, 5′-ACACCTCTGCTCAGACCTGAA-3′; and Px1ex4-R, 5′-TGCACAGAAACTCGTCCGAGA-3.

With these oligonucleotides, the Px1 band (336 bp, exon 3–4) was clearly visible in the WT mice but absent in Px1 KO mice. Genotyping for Px1 KO, Cx30 KO (1), and P2x7 KO mice (4) was also performed by standard PCR on extracted mouse tail tips. Primer pairs were specific for the WT alleles. Thus, the primers are as follows for Px1: wtin, 5′-GGAAAGTCAACAGAGGTACCC-3′; and wtex, 5′-CTTGGCCACGGAGTATGTGTT-3′. Primers for Cx30 were as follows: Cx30F, 5′-GGTACCTTCTACTAATTAGCTTGG-3′; and Cx30R, 5′-AGGTGGTACCCATTGTAGAGGAAG-3′. Primers for P2x7 were as follows: P2x7F, 5′-TGCCCATCTTCTGAACACC-3′; and P2x7R, 5′-CTTCCTCTTACTGTTTCCTCCC -3′.

To visualize the deletion, primers specific for the *lacZ* region (which flanks the deleted allele) were used in combination with the corresponding WT forward primer: Px1lac, 5′-GTCCCTCTCACCACTTTTCTTACC-3′; Cx30lac, 5′-AGCGAGTAACAACCCGTCGGATTC-3′; and P2x7lac, 5′-GCAAGGCGATTAAGTTGGG-3′.

Targeted ablation of Cx26 in the otic capsule was achieved by crossing $Cx26^{loxP/loxP}$ mice (2) with Sox10-Cre mice (3, 5). Double transgenic mice were detected by screening for the presence of the two insertions, *loxP* and *Cre*, by PCR on extracted mouse tail tips by using the following primers (see supplementary materials in ref. 2): Cx26F, 5′-CTTTCCAATGCTGGTGGAGTG-3′; Cx26R, 5′-ACAGAAATGTGTTGGTGATGG-3′; CreF, 5′-GCATTACCGGTCGATGCA-3′; and CreR, 5′-GAACCTGGTCGAAATCAG-3′.

Animal handling was approved by the Committee for Animal Care and Use of the University of Padua, Italy.

Immunohistochemistry and Confocal Imaging. For highly selective staining of the plasma membrane, cell cultures were incubated for 15 min at 37°C with 5 μg/ml red-fluorescent Alexa Fluor 594 wheat germ agglutinin (part number I34406; Invitrogen) diluted in PBS solution. Stained samples were fixed in 4% paraformaldehyde for 20 min at 4°C, but not permeabilized. To analyze connexin expression at the endolymphatic surface of the organ of Corti [supporting information (SI) Fig. S1], fixed preparations were incubated overnight at 4°C with primary polyclonal antibodies (Abs) directed against peptides corresponding to the extracellular loops of Cx26 (gift from Guy Tran Van Nhieu, Institut Pasteur, Paris, France) (6). After washing three times in PBS solution (5 min each time), secondary antibodies (Alexa Fluor 488 goat anti-rabbit IgG, part number A-11008; Invitrogen) were applied at 5 μg/ml for 1 h at room temperature. After washing for further three times in PBS solution, coverslips were mounted onto glass slides with anti-fade medium and analyzed using a Leica TCS SP5 confocal microscope equipped with a $\times$63 oil-immersion objective (NA 1.4, HCX PL APO). Alexa Fluor 488 was excited by the 488-nm line of an argon laser and its green fluorescence emission was collected in a spectral window between 495 nm and 540 nm. Alexa Fluor 594 was excited by the 543-nm line of a He-Ne laser and its red fluorescence emission was collected between 640 and 740 nm. Laser line intensities and detector gains were carefully adjusted so that no signal could be detected in the red emission window when scanning the samples at 488 nm; reciprocally, no signal was detected in the green emission window when scanning at 543 nm.

Ratiometric Ca^{2+} Imaging. For ATP stimulation experiments (*i*), organ cultures were incubated for 30 min at 37° in EXM supplemented with fura-2AM (16 μM). Alternatively, for photostimulation experiments (*ii*), cultures were incubated for 70 min with fura red AM (5 μM) and caged IP_3 AM (5 μM). In either case, the incubation medium also contained pluronic F-127 (0.01%, wt/vol) and sulfinpyrazone (250 μM) to prevent dye sequestration and secretion (7). For recording, cultures were transferred on the stage of an upright microscope (BX51; Olympus) and perfused in EXM for 20 min at 2 ml/min to allow for de-esterification.

For experiment (*i*), fura-2 fluorescence was excited alternatively at 360 nm and 380 nm by a fast-switching monochromator (Polychrome IV; Till Photonics) and directed onto the sample through a dichromatic mirror (470dcrx; Chroma). Fluorescence emission was selected at approximately 510 nm by using an interference filter (D510/40m; Chroma) to form fluorescence images on a scientific-grade CCD camera (SensiCam QE; PCO Computer Optics) using a $\times$20 water-immersion objective (NA 0.95; Lum Plan FL; Olympus). Baseline fluorescence emission was recorded for 10 s, and thereafter ATP (dissolved in DFM at the concentration of 4 μM) was focally applied from a glass micropipette with a tip opening of $\approx$1.5 μm and fluorescence was monitored for more than 1 min. In all experiments, the pipette was placed near the outer hair cell stereocilia and pressure was applied at its back by a Pneumatic PicoPump (PV800; World Precision Instruments) gated by a pulse of 50 ms under software control. Thus, by "ATP puff" we mean the

amount of ATP delivered to the culture when a 50-ms TTL pulse gated the pressure valve, with 4 μM ATP in the micropipette. To characterize this ATP delivery method (used in Fig. 1 of the main text), we measured the increasing time of a Ca^{2+} signal induced by an ATP puff, comparing it with the fluorescence signal obtained by loading the micropipettes with 4 μM fluorescein and applying the same pressure pulse to its back, after positioning the fluorescein-loaded pipette at the same location on the same culture (to obtain similar boundary conditions). The signal caused by fluorescein peaked in $\approx$100 ms after the end of the TTL pulse; in this time interval, fluorescein spread over an approximately circular area with a diameter of $\approx$100 μm. By contrast, the Ca^{2+} signal evoked by an ATP puff peaked in the first responding cells with a delay of $\approx$1 sec, when the corresponding fluorescein signal was already decaying exponentially as a result of diffusion.

For experiment (*ii*), fura red fluorescence was excited alternatively at 460 nm (isosbestic point) and 490 nm through a dichromatic mirror (515dcrx; Chroma). For the experiments reported in Figs. 2 and 5 and Fig. S5, cultures were observed with a $\times$60 water-immersion objective (N.A. 1.0, Fluor; Nikon) and emission was monitored with the CCD camera (Sensicam QE) through an emission filter (D660/50; Chroma). For IP_3 uncaging, the output of a TTL-controlled lased diode (10 mW, 375 nm, part number LD1489; Power Technology) was merged into the excitation light path via a UV transparent fiber-optic cable (0.22 N.A., 200 μm core; Rapp OptoElectronic). For UV illumination, fiber output was projected onto the specimen plane by a UV-grade fused silica collimating lens (25 mm effective focal length, part number G48–293; Edmund Optics) followed by a dichromatic mirror (400 dclp; Chroma) placed at 45° just above the objective lens of the microscope. By carefully adjusting the position of the fiber in front of the collimating lens, we maximized light intensity throughput while projecting a sharp demagnified image of the illuminated fiber core (i.e., spot) onto the specimen focal plane selected by the (infinity corrected) objective lens. Under these conditions, the fiber-optic diameter accurately determined the area of IP_3 photolysis, which encompassed few supporting cells. Because intense UV illumination can also damage cells and trigger ICS in the absence of caged IP_3 (8), we performed a series of preliminary control experiments to find the minimal UV dose sufficient for uncaging IP_3, and determined that it corresponds to a laser pulse duration of 100 ms. To establish a safety margin, we additionally verified that no Ca^{2+} signal was evoked by UV pulses as long as 2 s if caged IP_3 was omitted from the loading solution. During uncaging experiments, baseline fluorescence emission was recorded for 10 s, and thereafter a UV laser pulse of 100 ms was applied to release IP_3 and fluorescence emission was monitored for a maximum of 1 min.

For experiments (*i*) and (*ii*), image sequences were acquired by using software developed in the laboratory, stored on disk, and processed off-line as described (9, 10) using the Matlab 7.0 software package (MathWorks). Signals were measured as dye emission ratio changes, $\Delta R = R(t) - R(0)$, where t is time and $R(t)$ is emission intensity excited at 360 nm (fura-2) or 460 nm (fura red) divided by the intensity excited at 380 nm (fura-2) or 490 nm (fura red), and $R(0)$ indicates pre-stimulus ratio.

ATP Biosensors. ATP biosensors consisted of CHO cells transfected with rat P2x2 and P2x3 receptors (11). We separately loaded cochlear tissue with caged IP_3 AM and ATP biosensors with AM ester of the highly sensitive non-ratiometric Ca^{2+} indicator fluo-4. Thereafter we transferred the biosensors to the chamber holding the cochlear culture on the microscope stage. For each experiment, we selected a biosensor cell by initially applying 100 nM ATP and identifying responsive cells as described by Huang *et al.* (12). For IP_3 uncaging (Fig. 3), conditions were identical to those described earlier. For analysis, we computed whole-cell pixel averages of percent fluo-4 fluorescence change (ΔF) relative to pre-stimulus fluorescence emission intensity (F_0) measured before delivery of the photostimulation.

Calcein and Fluorescence Recovery After Photobleaching. Mouse cochlear cultures were incubated for 10 min at 37°C in EXM supplemented with 5 μM calcein-AM, 250 μM sulfinpyrazone, and 0.01 wt/vol pluronic F-127; transferred to the microscope stage; perfused for 20 min at 2 ml/min in EXM to allow for de-esterification; and thereafter maintained in still EXM at room temperature. Calcein fluorescence (Fig. 4 and Figs. S6 and S7) was excited at 488 nm through a dichromatic mirror (515dcrx; Chroma). Cultures were observed with the $\times$20 water-immersion objective (Olympus) and emission was monitored with the CCD camera (Sensicam QE) through an emission filter (HQ535/30m; Chroma). In all experiments, the effects of photobleaching from illumination at 488 nm were kept under control by carefully selecting the most appropriate inter-frame interval while controlling sample irradiation with a mechanical shutter triggered by the frame-valid signal of the CCD camera. Baseline fluorescence emission at 535 nm was recorded for 50 s, followed by focal laser irradiation at 375 nm for 2 s to bleach intracellular calcein (13, 14). Thereafter, fluorescence recovery after photobleaching (FRAP) was monitored for up to 600 s. For analysis of FRAP experiments (Fig. S7), we delineated a region of interest (ROI) inside the bleached area, plus a ROI in a proximal unbleached area, and we computed ratios of fluorescence intensities at each time point. For analysis of calcein efflux (Fig. 4 in the main text), we measured the time course of percent fluorescence emission change relative to initial fluorescence intensity.

Electrophysiology. For patch-clamp recordings from HeLa cells (Fig. S8), Ca^{2+} and/or La^{3+} were added to an extracellular medium containing (in mM): K aspartate 127.7, NaCl 5.4, $MgCl_2$ 1, Hepes 10, TEA 2, CsCl 2, $BaCl_2$ 2, pyruvate 2, glucose 5; pH 7.4, 320 mOsm. Patch pipettes were filled with a medium containing (in mM): K aspartate 120, NaCl 10, $CaCl_2$ 1, $MgCl_2$ 1, Mg ATP 3, Hepes 5, EGTA 10; pH 7.2, 320 mOsm. For other methodological details (cell culture, transfection and recording) see refs. 15 and 16.

1. Teubner B, *et al.* (2003) Connexin30 (Gjb6)-deficiency causes severe hearing impairment and lack of endocochlear potential. *Hum Mol Genet* 12:13–21.
2. Cohen-Salmon M, *et al.* (2002) Targeted ablation of connexin26 in the inner ear epithelial gap junction network causes hearing impairment and cell death. *Curr Biol* 12:1106–1111.
3. Matsuoka T, *et al.* (2005) Neural crest origins of the neck and shoulder. *Nature* 436:347–355.
4. Sim JA, Young MT, Sung HY, North RA, Surprenant A (2004) Reanalysis of P2X7 receptor expression in rodent brain. *J Neurosci* 24:6307–6314.
5. Watanabe K, *et al.* (2000) Expression of the Sox10 gene during mouse inner ear development. *Brain Res Mol Brain Res* 84:141–145.
6. Clair C, Combettes L, Pierre F, Sansonetti P, Tran Van Nhieu G (2008) Extracellular-loop peptide antibodies reveal a predominant hemichannel organization of connexins in polarized intestinal cells. *Exp Cell Res* 314:1250–1265.
7. Di Virgilio F, Steinberg TH, Silverstein SC (1990) Inhibition of Fura-2 sequestration and secretion with organic anion transport blockers. *Cell Calcium* 11:57–62.
8. Gale JE, Piazza V, Ciubotaru CD, Mammano F (2004) A mechanism for sensing noise damage in the inner ear. *Curr Biol* 14:526–529.
9. Bastianello S, Ciubotaru CD, Beltramello M, Mammano F (2004) Dissecting key components of the Ca2+ homeostasis game by multi-functional fluorescence imaging. *Proc SPIE* 5324:265–274.
10. Piazza V, Ciubotaru CD, Gale JE, Mammano F (2007) Purinergic signalling and intercellular Ca2+ wave propagation in the organ of Corti. *Cell Calcium* 41:77–86.
11. Kawashima E, *et al.* (1998) A novel and efficient method for the stable expression of heteromeric ion channels in mammalian cells. *Receptors Channels* 5:53–60.
12. Huang YJ, *et al.* (2007) The role of pannexin 1 hemichannels in ATP release and cell-cell communication in mouse taste buds. *Proc Natl Acad Sci USA* 104:6436–6441.

13. Wade MH, Trosko JE, Schindler M (1986) A fluorescence photobleaching assay of gap junction-mediated communication between human cells. *Science* 232:525–528.
14. Rabut G, Ellenberg J (2005) Photobleaching techniques to study mobility and molecular dynamics of proteins in live cells: FRAP, iFRAP, and FLIP. *Live Cell Imaging*, ed Goldman RD, Spector DL (Cold Spring Harbor Lab Press, Cold Spring Harbor, NY), pp 101–126.
15. Beltramello M, *et al.* (2003) Permeability and gating properties of human connexins 26 and 30 expressed in HeLa cells. *Biochem Biophys Res Commun* 305:1024–1033.
16. Hernandez VH, *et al.* (2007) Unitary permeability of gap junction channels to second messengers measured by FRET microscopy. *Nat Methods* 4:353–358.

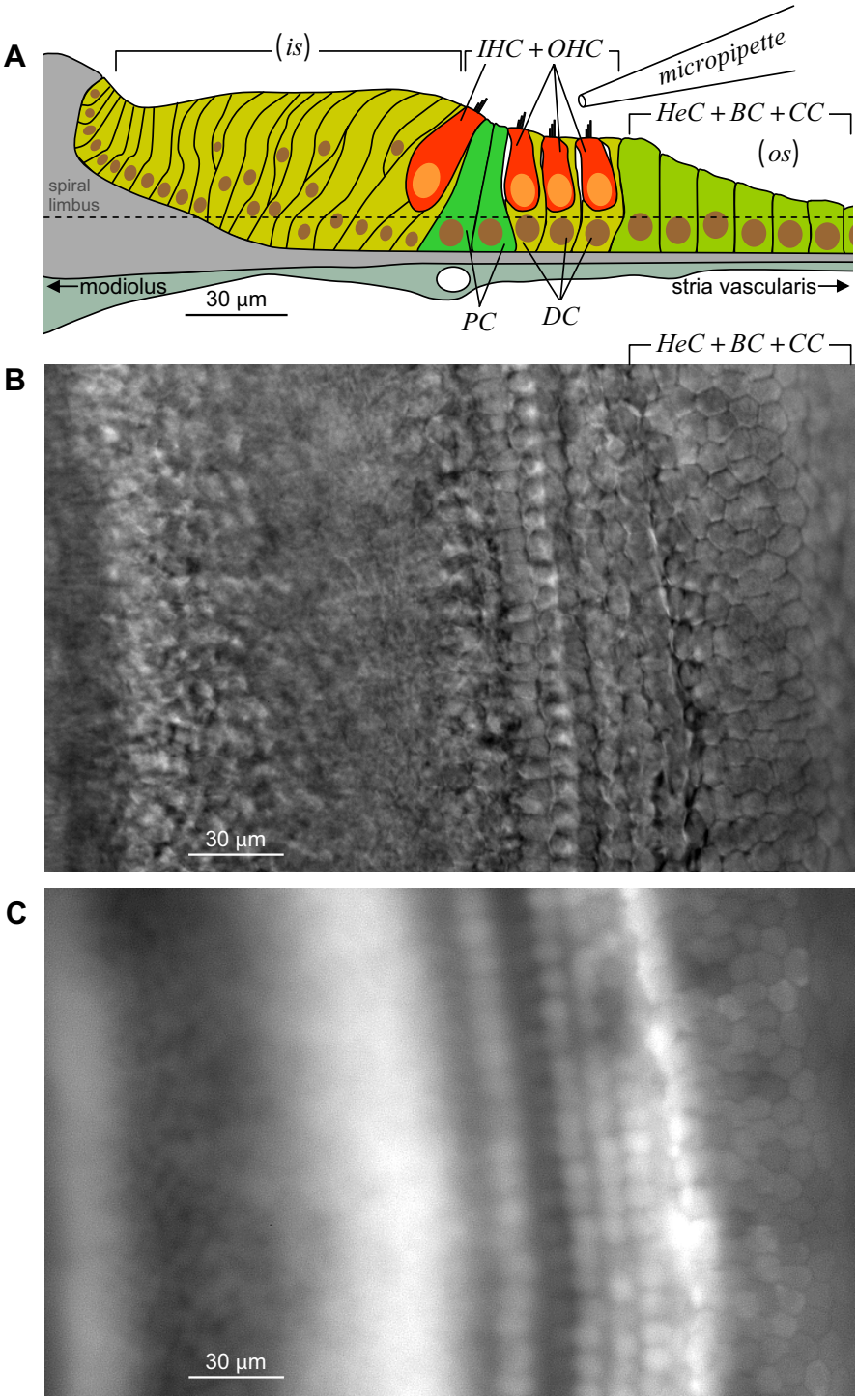

Fig. S1. Cochlear organotypic culture. (*A*) Schematic view of the sensory epithelium in a transverse section of a mouse organotypic culture. The diagram is based on the thin-section photomicrograph in figure 1b of Russell IJ, Richardson GP (1987) The morphology and physiology of hair cells in organtypic cultures of the mouse cochlea. *Hear Res* 31:9–24. The region between the outer hair cells (OHC) and the stria vascularis comprises supporting and epithelial cells known as Hensen's (HeC), Böttcher's (BC), and Claudius' cells (CC); we shall refer broadly to this region as the outer sulcus (os). In the adult, the region between the inner hair cell and the spiral limbus hosts other non-sensory cells (e.g., phalangeal cells, inner border cells, and inner sulcus cells; for detailed anatomical description, see ref. 1 in the main text), whereas in the developing cochlea it is occupied by the wide expanse of columnar-shaped supporting cells of the Köllicher organ (see refs.10 and 38 in the main text); we shall refer broadly to this region as the inner sulcus (is). Other labeled cells in the diagram are pillar cells (PC) and Deiters' cells (DC). The position of the glass micropipette used to deliver ATP is also shown. (*B*) Differential interference contrast and (*C*) corresponding wide-field fura-2 fluorescence micrograph show top views through the same region of a living culture; the approximate location of the focal plane in *B* and *C* is indicated by the horizontal dashed line in *A*.

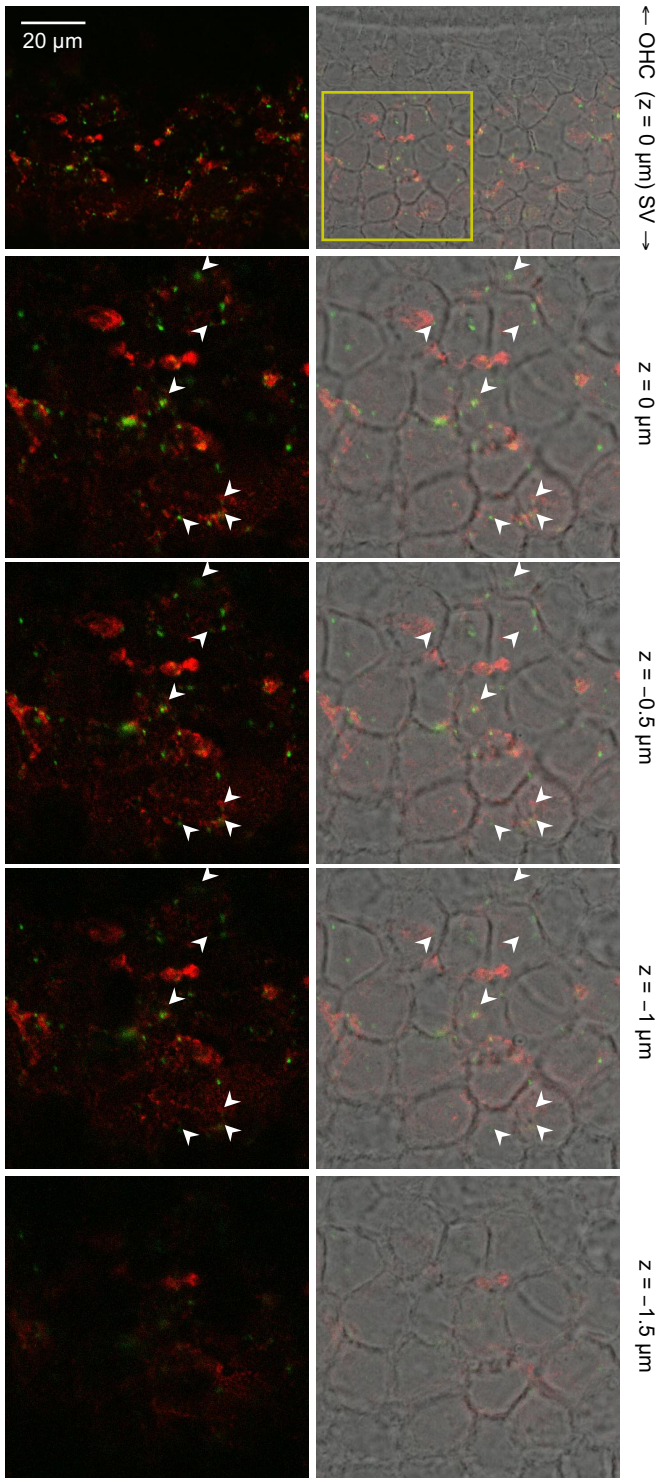

Fig. S2. Connexin immunoreactivity near the endolymphatic surface of the organ of Corti. Through focus confocal image sequence (z-stack) of cochlear supporting and epithelial cells in the region comprised between outer hair cells (OHC) and stria vascularis (SV), immuno-labeled with Abs directed against peptides corresponding to the extracellular loops of Cx26 (primary antibodies) and green-fluorescent secondary antibodies. Cell plasma membranes in these fixed, but non-permeabilized, preparations were stained with red-fluorescent wheat germ agglutinin. *Left*, merged green and red channels. *Right*, overlay of *Left* images on the corresponding grayscale transmitted light differential interference contrast images. Arrowheads points to apical plasma membrane Cx26 signals from locations that, *in vivo*, would be exposed to endolymph.

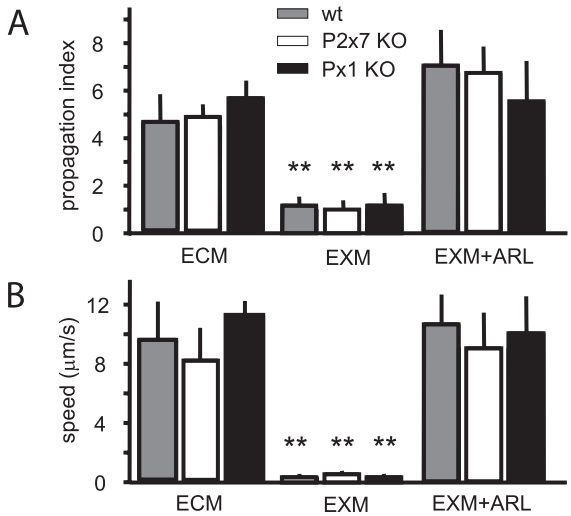

Fig. S3. WT, Px1 KO and P2x7 KO cultures are similarly sensitive to extracellular Ca^{2+} and ectonucleotidase activity. Pooled data showing propagation index (*A*) and speed (*B*) of ICS evoked by photostimulation of cochlear supporting cells from controls (WT) and cultures lacking (KO) P2x7 or Px1. EXM, extracellular medium containing 2 mM Ca^{2+}; ECM, medium containing endolymphatic Ca^{2+} concentration (20 μM); EXM+ARL, ectonucleotidase inhibitor ARL67156 (100 μM) dissolved in EXM. Data are mean ± SE for independently repeated experiments in tissues from at least three different animals.

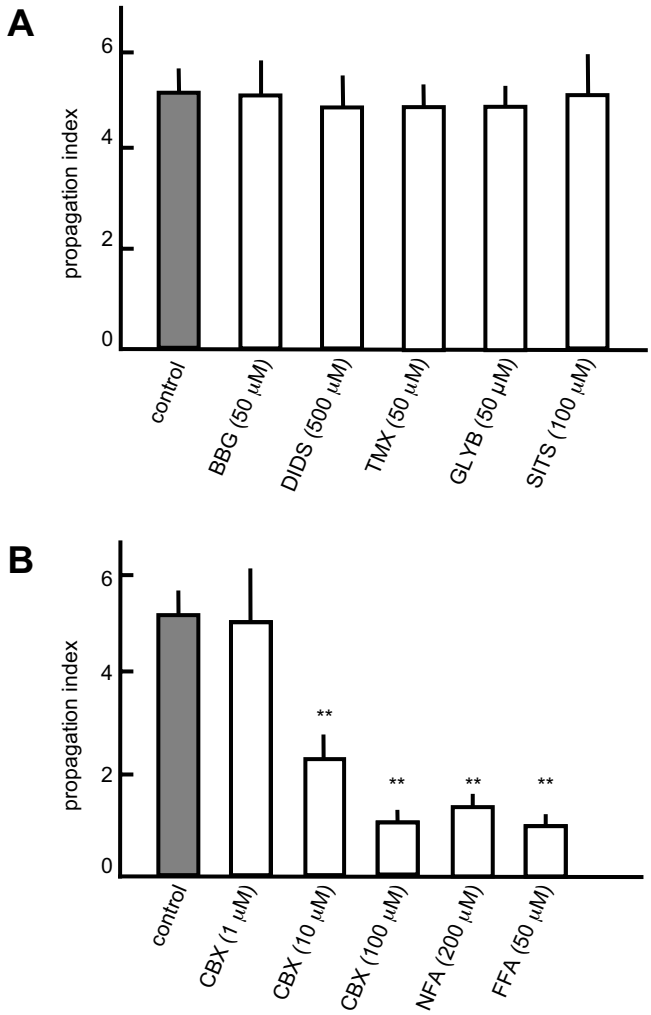

Fig. S4. Connexin channel blockers inhibit ICS propagation in the organ of Corti. Sensitivity of ICS propagation index to pharmacological inhibition in cultures from WT mice incubated with (*A*) brilliant blue G (BBG), 4,4′-di-isothiocyanatostilbene-2,2′-disulfonic acid (DIDS), tamoxifen (TMX), glybenclamide (GLYB), 4-acetamido-4′-isothiocyanostilbene-2′,2-disulfonate (SITS); or (*B*) carbenoxolone (CBX), niflumic acid (NFA), or flufenamic acid (FFA). Data are mean ± SE for independently repeated experiments on cultures from at least four different animals.

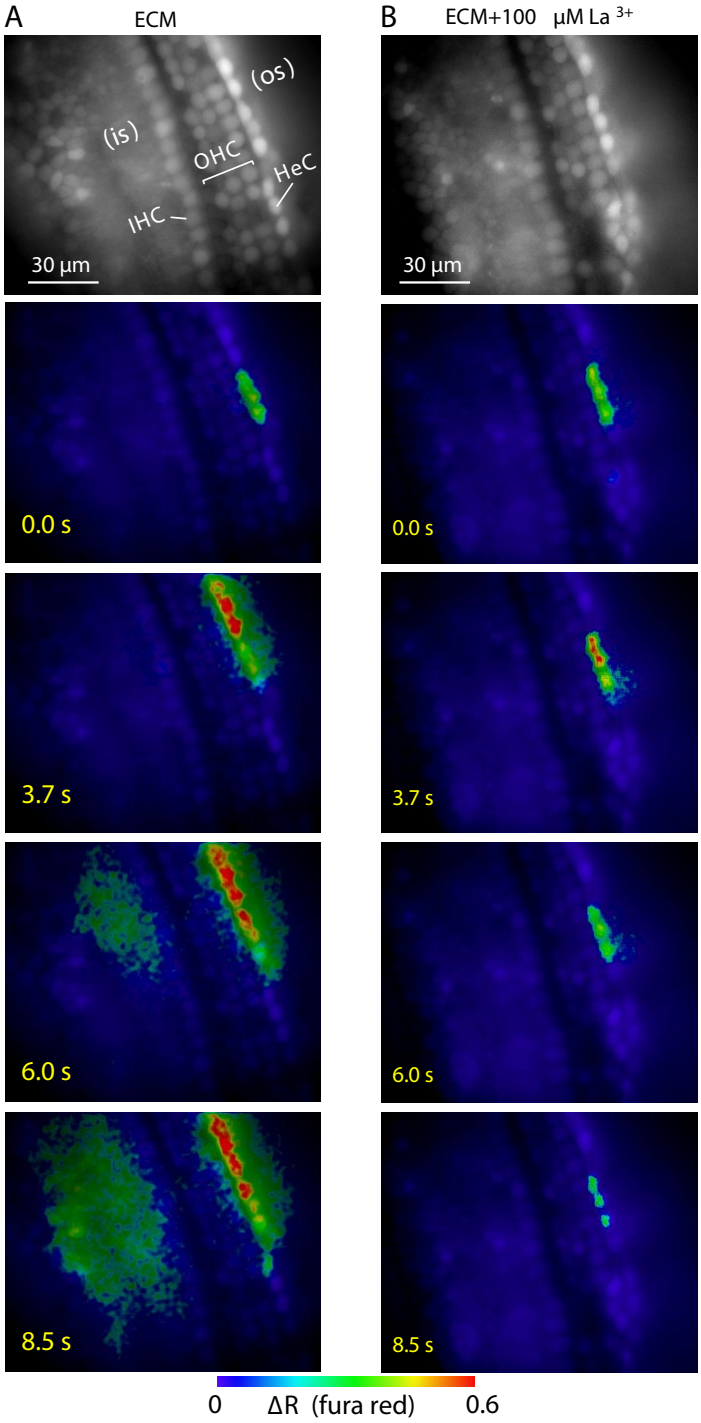

Fig. S5. ATP release from cochlear supporting cells affords a communication pathway across the sensory hair cell region. (*A*) *Top*, fura red fluorescence image of a cochlear culture bathed in ECM and co-loaded with the AM esters of fura red and caged IP_3, showing location of supporting cells on both sides of the sensory hair cell region (for acronyms, see Fig. S1). The other frames show Ca^{2+} signals, represented as pseudo-color images, evoked by 100 ms of focal UV photolysis of caged IP_3. Time of image capture, measured from the end of stimulus, is indicated on the bottom left corner of each frame. (*B*) Same as *A* for a different field of the same culture exposed to 100 μM La^{3+} to block connexin hemichannels.

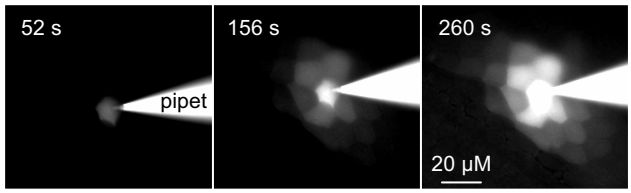

Fig. S6. Calcein permeates across intercellular GJ channels in the organ of Corti. Sequence of fluorescence images from a representative experiment showing delivery of calcein, under gigaseal whole-cell patch-clamp conditions, from a glass micropipette to a selected supporting cell, followed by dye spreading to neighboring cells in a region between the OHCs and the stria vascularis of a WT mouse culture bathed in EXM. Time of image capture, measured from the onset of microinjection, is indicated on the top left corner of each frame.

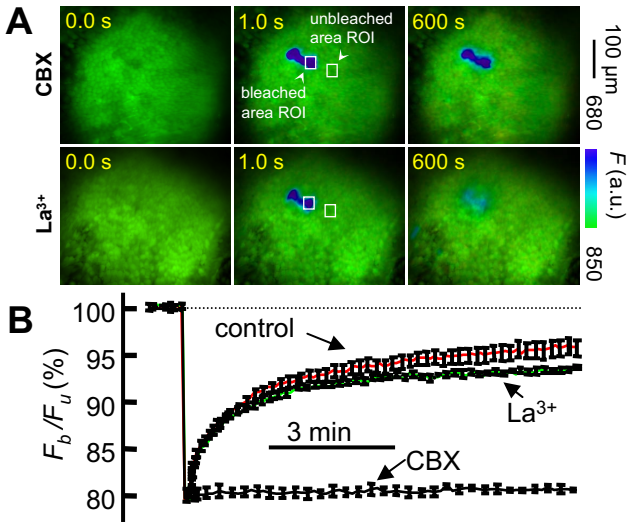

Fig. S7. Effects of CBX and La^{3+} on calcein FRAP in the organ of Corti. (*A*) FRAP processes in WT cultures preloaded with calcein AM and exposed to 100 μM CBX (*Top*) or 100 μM La^{3+} (*Bottom*). Calcein fluorescence intensity (*F*), in arbitrary units (a.u.), is mapped to pseudo-colors as indicated by the color-scale bar (bright green represents basal dye fluorescence). (*B*) ROI fluorescence intensities ratios F_b/F_u (i.e., bleached area/unbleached area) versus time for WT cochlear cultures in control conditions (red line) and following incubation for 30 min with 100 μM La^{3+} (green line) or 100 μM CBX (black line) in five independent experiments for each condition. Error bars indicate SEM.

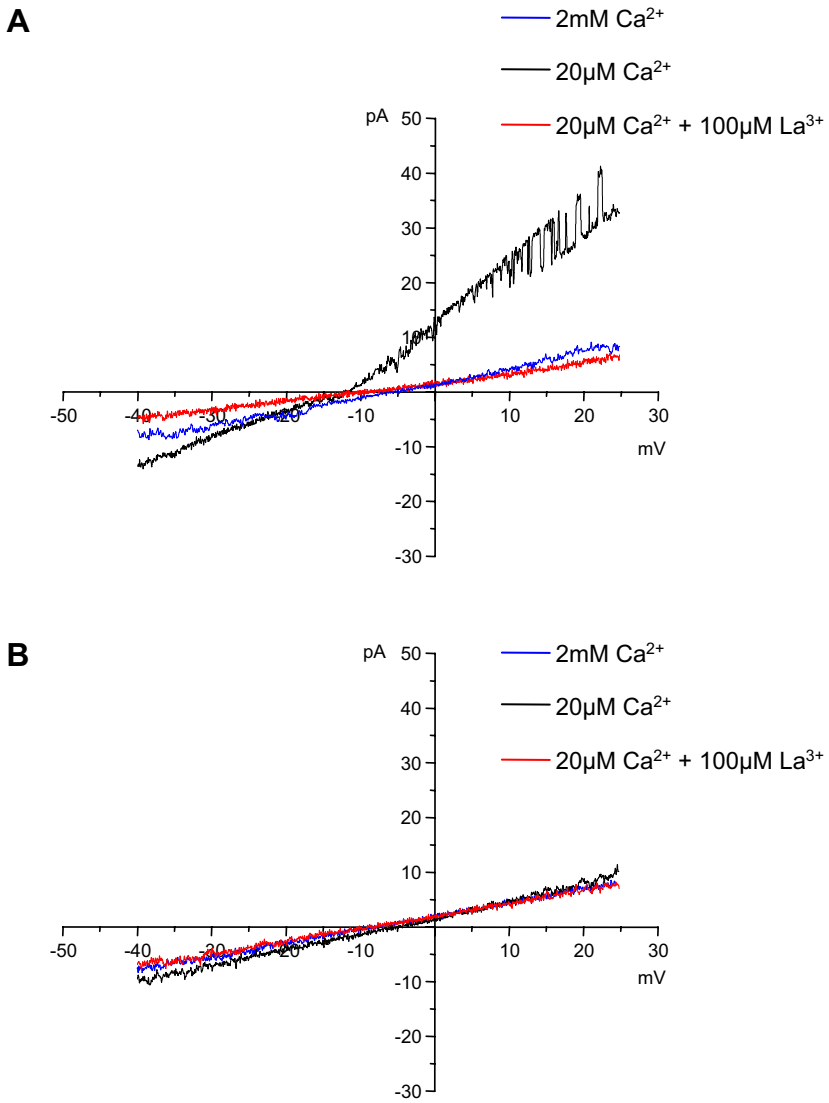

Fig. S8. Action of La^{3+} on currents evoked by depolarization in patch-clamped solitary HeLa cells. (*A*) Three representative responses to voltage ramps obtained from the same HeLa cell transiently transfected with mouse Cx30, first under control conditions with 2 mM Ca^{2+} in the superfusion medium (blue), then with 20 μM Ca^{2+} (black); note hemichannel openings at positive potentials, and their complete blockade with 100 μM La^{3+} in the 20 μM Ca^{2+} medium (red). (*B*) Same as *A* for a representative parental (un-transfected) HeLa cell.

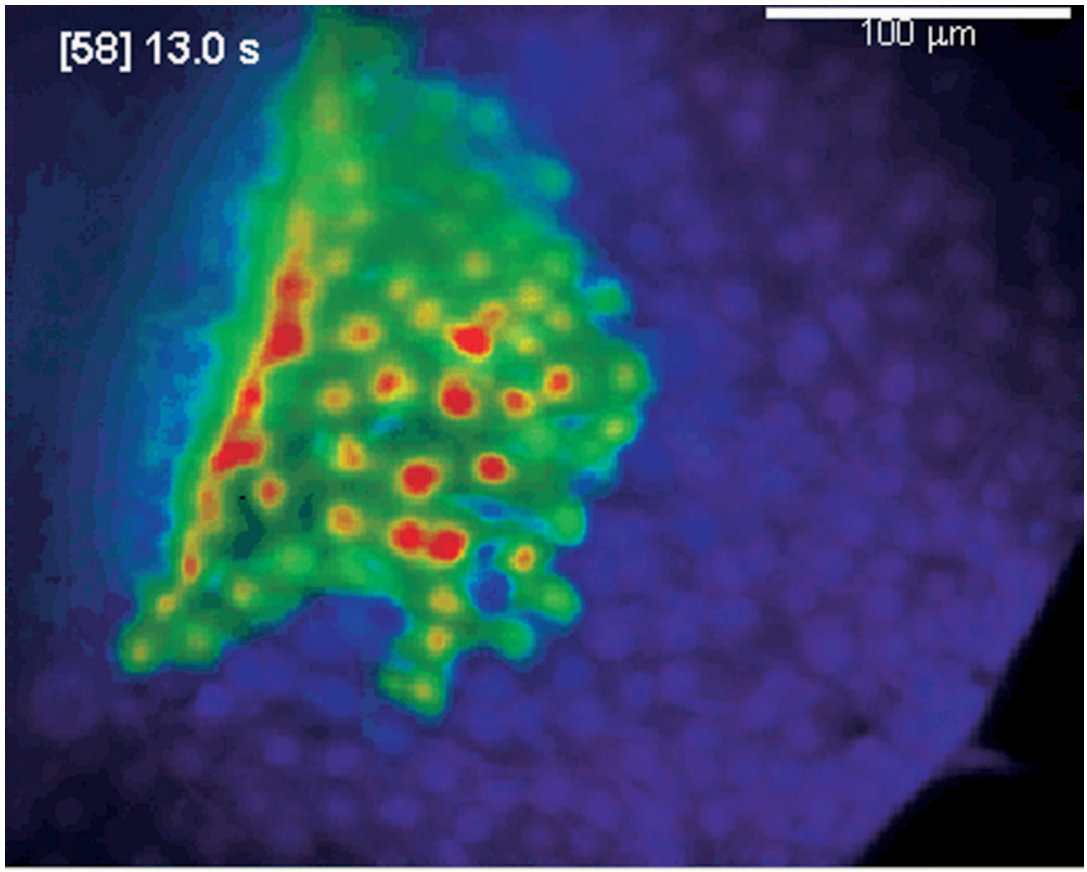

Movie S1. Ca^{2+} signals propagate across supporting cells in a cochlear organotypic culture from a wild type mouse, following focal delivery of an ATP puff from a micropipette opening positioned at the level of outer hair cells.

Movie S1 (AVI)

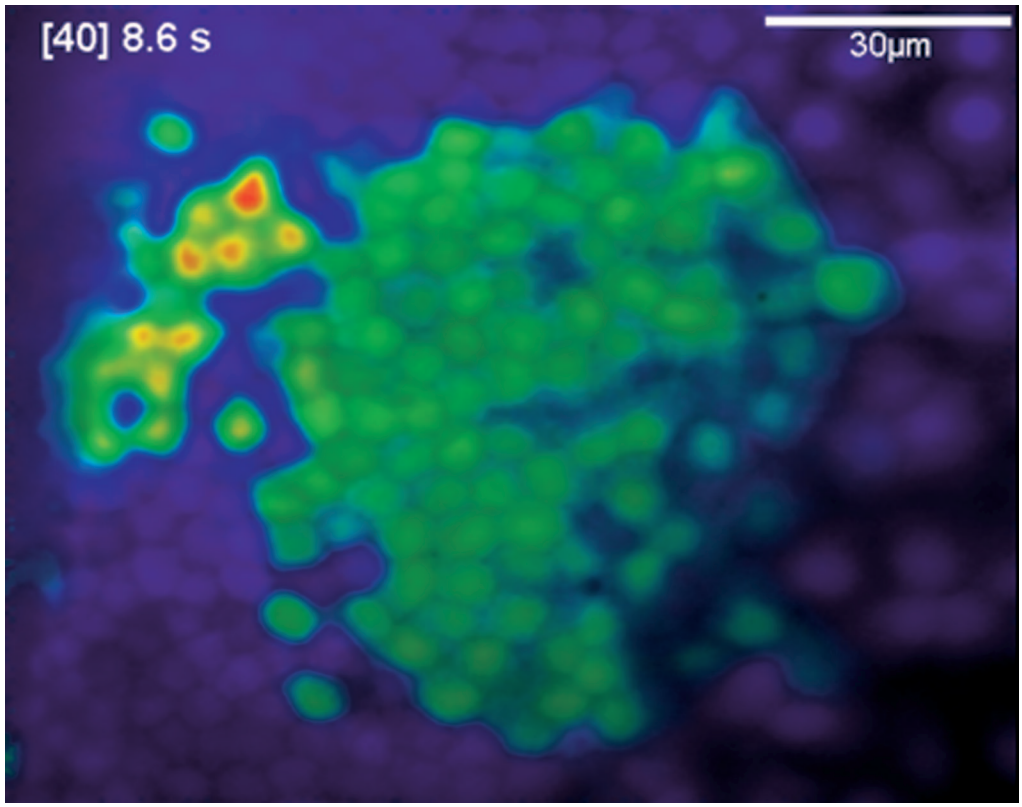

Movie S2. Ca^{2+}signals propagate across supporting cells in a cochlear organotypic culture from a wild type mouse, following photostimulation with caged IP_3.

Movie S2 (AVI)

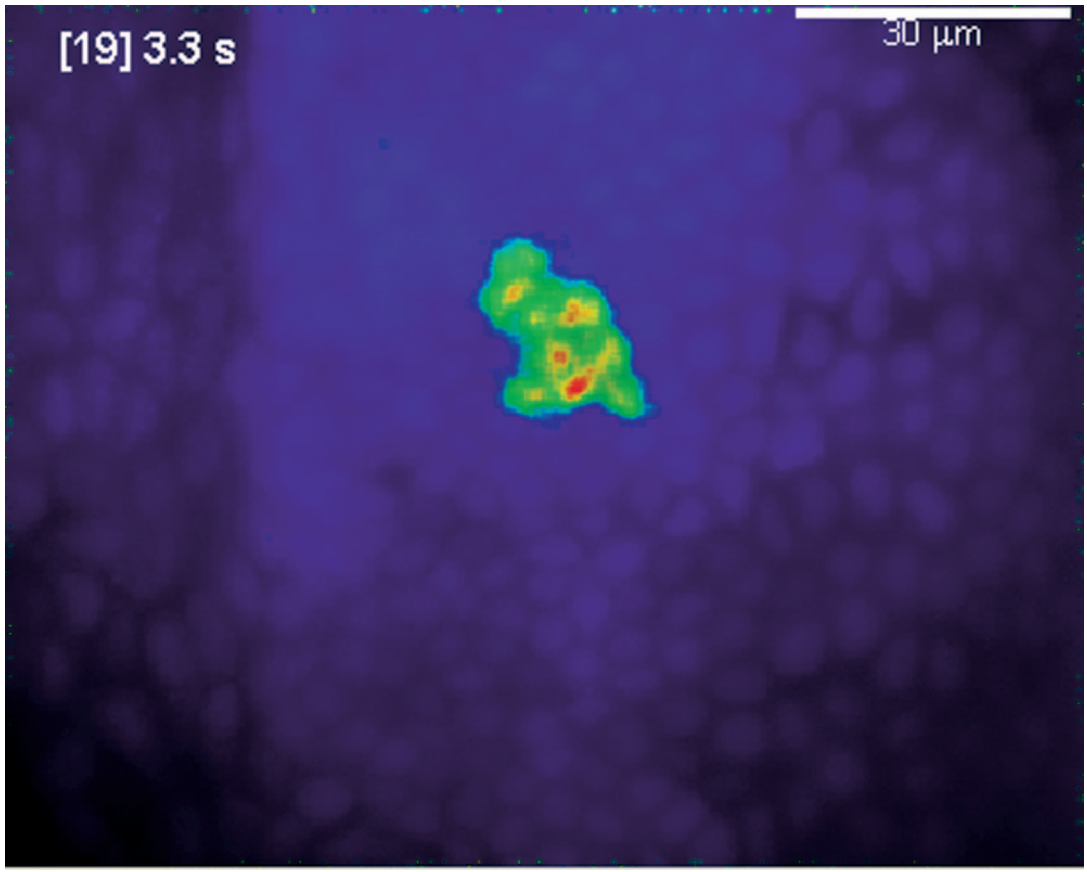

Movie S3. Ca^{2+}signals evoked by photostimulation with caged IP_3 fail to propagate in a connexin 26 deficient mouse culture.

Movie S3 (AVI)

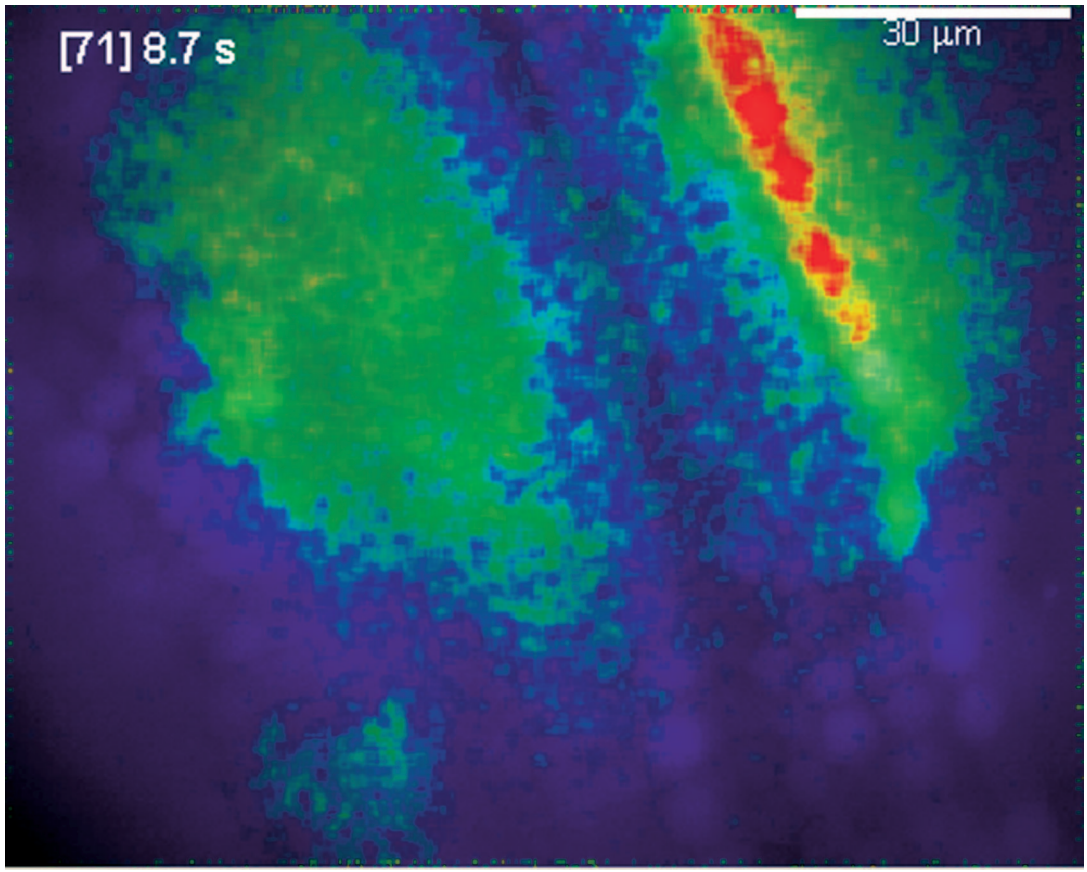

Movie S4. Ca^{2+} signals evoked by photostimulation with caged IP_3 in Hensen's cells propagate across the sensory hair cell region to cells of the Kölliker organ in a cochlear organotypic culture from a wild type mouse.

Movie S4 (AVI)